Journal of Visualization, Vol. 4, No. 3 (2001) 257-265

Velocity Field Measurements of Swirl Flow around a Forward-swept Axial Fan Using a Phase-averaged PTV

Lee, S. J.*1, Choi, J.*2 and Lee, I. S.*2

*1 Department of Mechanical Engineering, Pohang University of Science and Technology, Pohang 790-784, Korea.
*2 Digital Appliance Research Laboratory, LG Electronics, Seoul 153-023, Korea.

Received 21 March 2001.
Revised 12 July 2001.

***Abstract*:** The flow characteristics around a rotating axial fan were experimentally investigated using a phase-averaged PTV velocity field measurement technique. The axial fan has 5 forward-swept blades with a radius of 25 mm. Measurements were carried out at 4 axial planes and 4 radial planes perpendicular to the axis of rotation. For the axial plane measurements, one fan blade was divided into 4 different phases in order to analyze the flow structure according to blade phase. For each case, 500 instantaneous velocity fields were measured and ensemble averaged to obtain phase-averaged velocity vector fields and vorticity contours. In addition, measurements were carried out at two planes around the blade surface. Phase averaged velocity fields show periodic variations with respect to the blade phase. The periodic shedding of the tip vortex at the blade tip is also observed. The phase averaged velocity fields measured in the radial planes show periodic variations according to the fan phase and the distance from the fan. These experimental results can be used to validate numerical calculations and to understand the flow characteristics of forward-swept axial fans.

***Keywords*:** PTV, axial-fan, velocity field, phase-average, swirl flow, vorticity.

1. Introduction

Axial-fans have been used in various applications ranging from small home appliances to large fans used in industrial sites. However, they generate acoustic noise in some appliances. In order to improve the fan efficiency and reduce the acoustic noise generated in the operation of axial fans, accurate measurements of flow field around the fan is not only essential, but also indispensable for future developments of different kinds of turbomachinery. Since the fan wake is a complicated three-dimensional flow, however, it is not easy to analyze the flow through theoretical and numerical means, leading experimental researches on axial fans (Reynolds and Lakshminarayana, 1979).

Experimental studies on axial turbomachinery have had difficulties in analyzing the flow structure due to the lack of effective measurement instruments. Most previous studies measured the flow velocities at discrete points using point-wise measurement techniques. Ravindranath and Lakshminarayana (1980) measured the flow velocity in the wake of a compressor rotor blade using a tri-axial hot-wire probe rotating with the rotor. They revealed that large velocity decay occurs at the trailing edge of the blade and that the wake width in the trailing edge region varies rapidly.

Morris et al. (1998) investigated the velocity distribution in the wake of an automotive cooling fan using hot-wire anemometry. In general, hot-wire anemometry causes large errors in the reverse flow region such as just behind the fan. They confirmed the periodic variation of the fan wake according to the fan blade phase. Inoue and Kuroumaru (1984) measured the flow around a compressor rotor using a slanted hot-wire probe and the ensemble

averaging technique. They analyzed the vortex structure including the trailing vortex shed at the trailing edge of the rotor blade and the tip vortex shed from the outmost tip of the rotor blade.

Recently, field measurement techniques have been applied on the measurements of turbomachinery such as fans and pumps. Sinha and Katz (1998) used an auto-correlation PIV technique with a high-resolution CCD camera to measure the velocity fields inside a centrifugal pump. Cotroni et al. (2000) investigated the near wake of a marine propeller in a cavitation tunnel using PIV method.

There are few publications pertaining the measurement of velocity field of the flow around an axial fan. Most previous studies have dealt with axial rotors that are largely different in shape to that of the axial fan tested in this study.

2. Experimental Apparatus and Method

The axial fan has 5 forward-swept blades. The tip-to-tip diameter and the hub diameter of the fan are 50 mm and 14.3 mm, respectively, giving a hub-to-tip ratio of 0.286. The axial fan was installed inside a rectangular basin as shown in Fig. 1. An AC induction motor was used with an rpm controller for precise control of the fan rotation speed. The basin was made of transparent acrylic plate and a lid covering the upper surface was attached to eliminate the free surface effect. Tap water was used as the working fluid in which small particles having an average diameter of 37 μm and a specific gravity of 1.016 were seeded. The rotation speed of the axial fan was set at a constant 240 rpm throughout the experiments. A preliminary flow visualization experiment was carried out before the actual PTV measurements, using the same seeding particles. No distinct flow was observed in the vicinity of the basin walls.

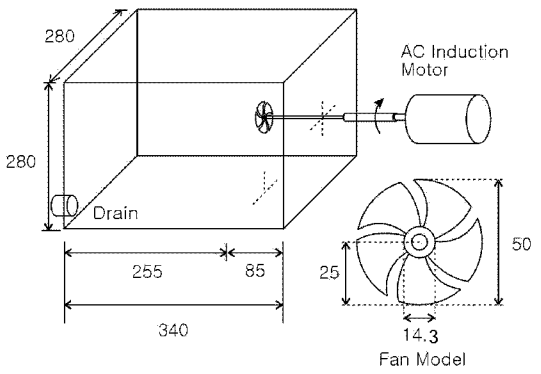

Fig. 1. Experimental setup and axial fan (units: mm).

The 2-frame PTV velocity field measurement system consists of a Nd:YAG laser, a high-speed CCD camera, a synchronization circuit and a PC as shown in Fig. 2. The dual-head Nd:YAG laser has a pulse width of 7 ns with a pulse rate of 20 Hz for each head. The high-speed CCD camera (SpeedCam^{+}) can capture particle images at a frame rate ranging from 31 Hz to 1 kHz at 1 Hz increments with 512×512 pixel resolution. Details of the synchronization circuits are described in Lee and Lee (1999).

A laser light sheet of approximately 2 mm in thickness was used to illuminate the measurement planes and to capture particle images for velocity field measurements. The measurement sections in the axial and radial planes are shown in Fig. 3. Velocity field measurements in the axial plane were carried out at 4 phases. The field of view is 40×40 mm^2, for which the lower-left corner was set at the center of the fan model ($z = 0$, $r = 0$). The 4 measurement phases were placed at angular intervals of 18° from the trailing edge of the blade tip and labeled as phases 1, 2, 3 and 4. The phase difference of 18° between two adjacent measurement phases corresponds to the elapse time of 12.5 ms. In addition, two additional measurement planes were selected for flow analysis around the blade surface (Fig. 3(b)). The mid-plane was located at the mid-span of the blade, and the tip-plane was located at the outmost tip of the blade, both parallel to the axis of rotation. The time interval between two consecutive particle images was set to $\Delta t = 1$ ms, for which the fan rotates 1.44° and the displacement of the blade tip is about 0.63 mm.

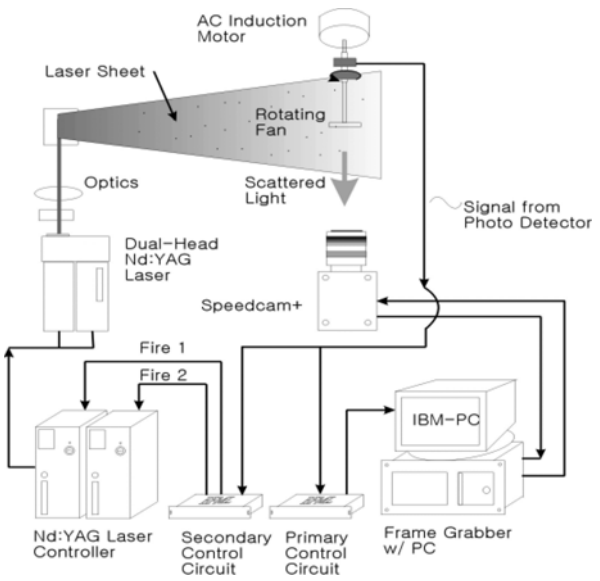

Fig. 2. Schematics of PTV system.

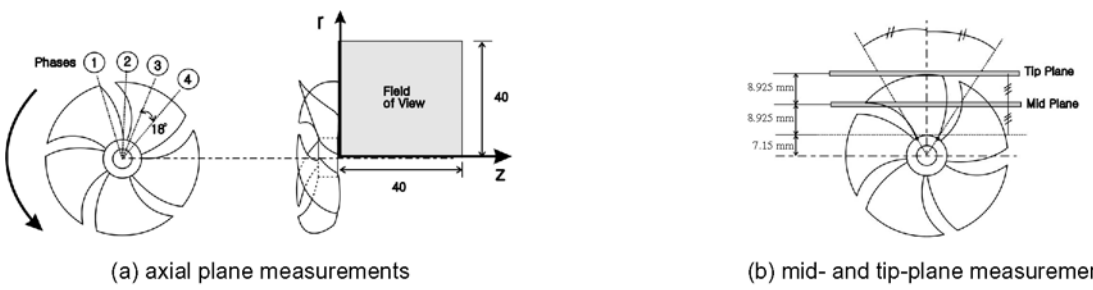

(a) axial plane measurements (b) mid- and tip-plane measurements

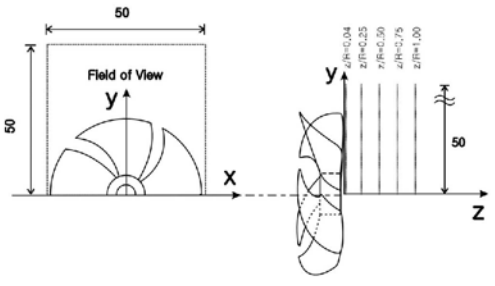

(c) radial plane measurements

Fig. 3. Field of views and coordinate system for axial and radial plane measurements (units: mm).

The coordinate axes and the field of view for radial plane measurements are shown in Fig. 3(c). Velocity field measurements were carried out at five upper-half planes perpendicular to the axis of rotation at distances of $z/R = 0.04$, 0.25, 0.5, 0.75 and 1. Due to larger field of view compared with the axial plane measurements, the time interval between two consecutive particle images was set at $\Delta t = 0.8$ ms, for which the fan rotates 1.15° and the tangential displacement at the blade tip is about 0.5 mm.

For each measurement section in the axial and radial planes, 1000 flow images were obtained. For the derivation of velocity field from captured particle images, a home-made 2-frame PTV algorithm based on match probability was applied. The 2-frame PTV algorithm has showed a better performance than conventional multi-

frame PTV methods in terms of computation time, recovery rate of correct velocity vectors, number of error vectors and dynamic range (Baek and Lee, 1996). The difference of mean velocity data between the 2-frame PTV method and LDV under the same flow conditions was found to be less than 1%. The instantaneous velocity vectors at random particle locations were interpolated into a regular grid using a multi-quadrant interpolation method. The phase-averaged mean velocity field was obtained by ensemble averaging the 500 instantaneous velocity fields at each case.

3. Results and Discussion

3.1 Axial Planes

500 instantaneous velocity vector fields measured for each of the 4 phases of the axial fan were ensemble averaged to give a phase-averaged mean velocity field. The abscissa and the ordinate of all results are represented z and r axes, normalized by the fan radius R. Figure 4 shows the ensemble-averaged mean velocity vector fields according to the fan phase (1 ~ 4). These phase-averaged velocity fields clearly show the periodic change of flow structure behind the axial fan. Figure 4(a) represents the mean velocity field measured at phase 1. A relatively high-momentum flow toward the hub is observed in the region just behind the fan (z/R<0.5), whereas the dominant flow in phases 2 and 3 is parallel to the axis of rotation. As the fan rotates through phase 4, the high-momentum flow is directed toward the hub again.

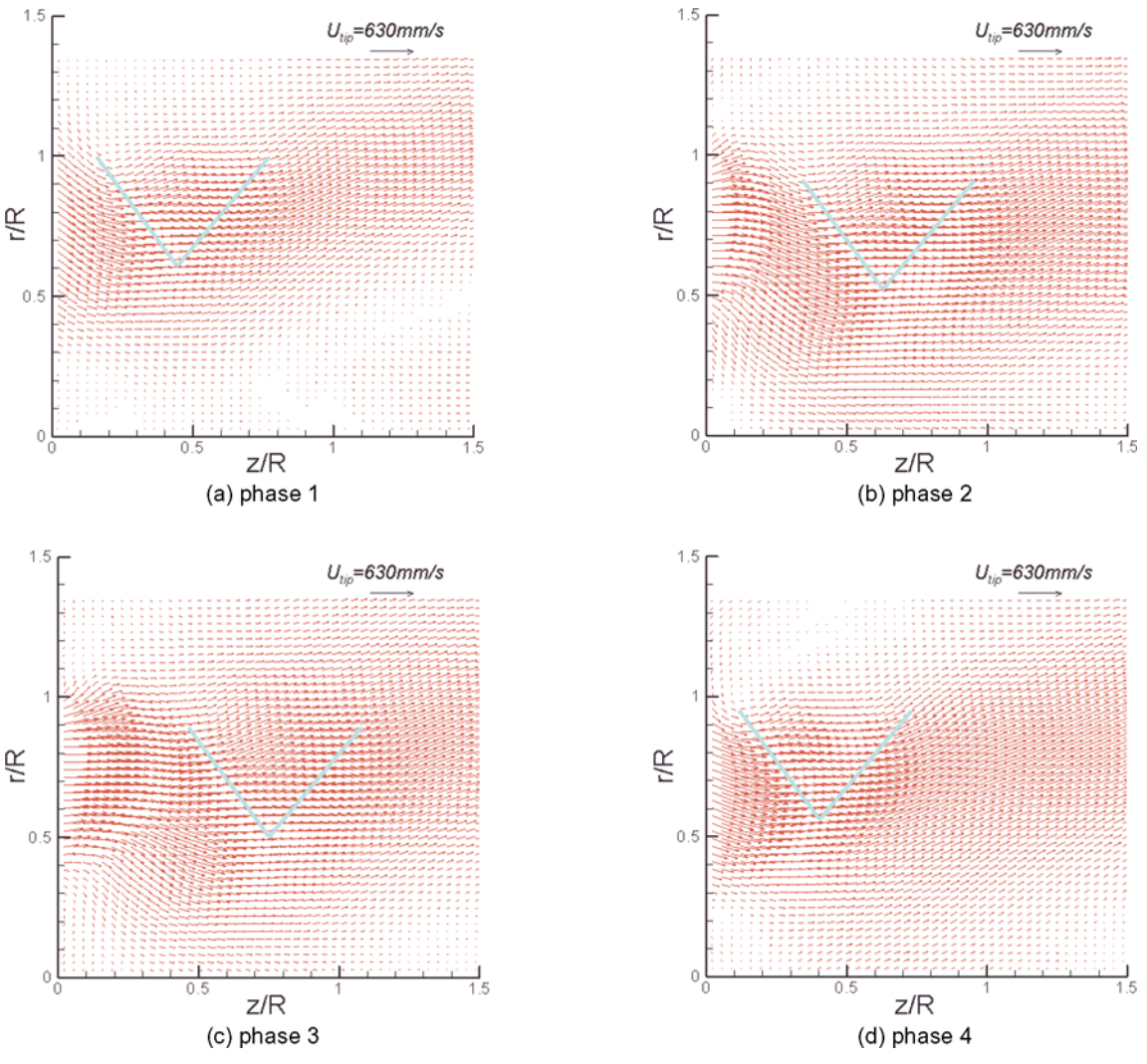

Fig. 4. Mean velocity vector fields in the axial plane.

The flow structure in the axial plane can be divided into 3 regions; the immediate wake region where the flow is directed toward the axis of rotation, the region where the flow is directed away from the axis of rotation, and the region thereafter the flow ceases to fluctuate. These seem to be closely related to the tip and trailing vortices. The dividing boundary where the flow is parallel to the axis of rotation can then be used to distinguish the different flow regions. The boundary in the velocity field of phase 1 shows a V shape, which is symmetric with respect to the vertical line $z/R = 0.43$. The vertical centerline is then shifted to the downstream location of $z/R = 0.61$ in phase 2. In phase 3, the V shaped boundary is observed at a further downstream location. However, the right half of the dividing boundary can no longer be clearly distinguished. This blurring of the dividing boundary results from the dissipation of the tip and trailing vortices as the flow goes downstream. This trend is shown for all blade phases tested in this study.

In Fig. 4(d) of phase 4, the flow structure is similar to that of phase 1, however, the V shaped boundary is located a small distance upstream in comparison with phase 1. The absolute value of the exit velocity at $z/R = 0$ is increased as the fan rotates from phase 1 to phase 4. In far wake region of $0.8<z/R$, the general flow structure remains constant regardless of the fan phase. From this, we can see that the fan phase only affects the flow in the vicinity of the fan blades where $z/R<0.8$. From these results, the periodic characteristics of the flow with respect to the fan phases can be observed.

Figure 5 shows the vorticity contours derived from the phase-averaged velocity field data. From these results, the shedding of the tip and trailing vortices were confirmed. In phase 1, a positive tip vortex is located behind the blade tip region. A region of negative vorticity exists between the hub and the mid-section of the fan blade. In this region, vortices of circular shape are difficult to find. In phase 2, however, a large-scale negative vortex rotating clockwise direction is shed from the blade in the region $0<z/R<0.2$, $0.4<r/R<0.8$. The positive tip vortex is moved downstream and its center is shifted from $z/R = 0.17$ to $z/R = 0.25$. At phase 3, the negative trailing vortex near the hub is increased in size and is transferred downstream. The center location of the vortices moves toward the axis of rotation from $r/R = 0.55$ in phase 2 to $r/R = 0.45$ in phase 3, while a new positive vortex

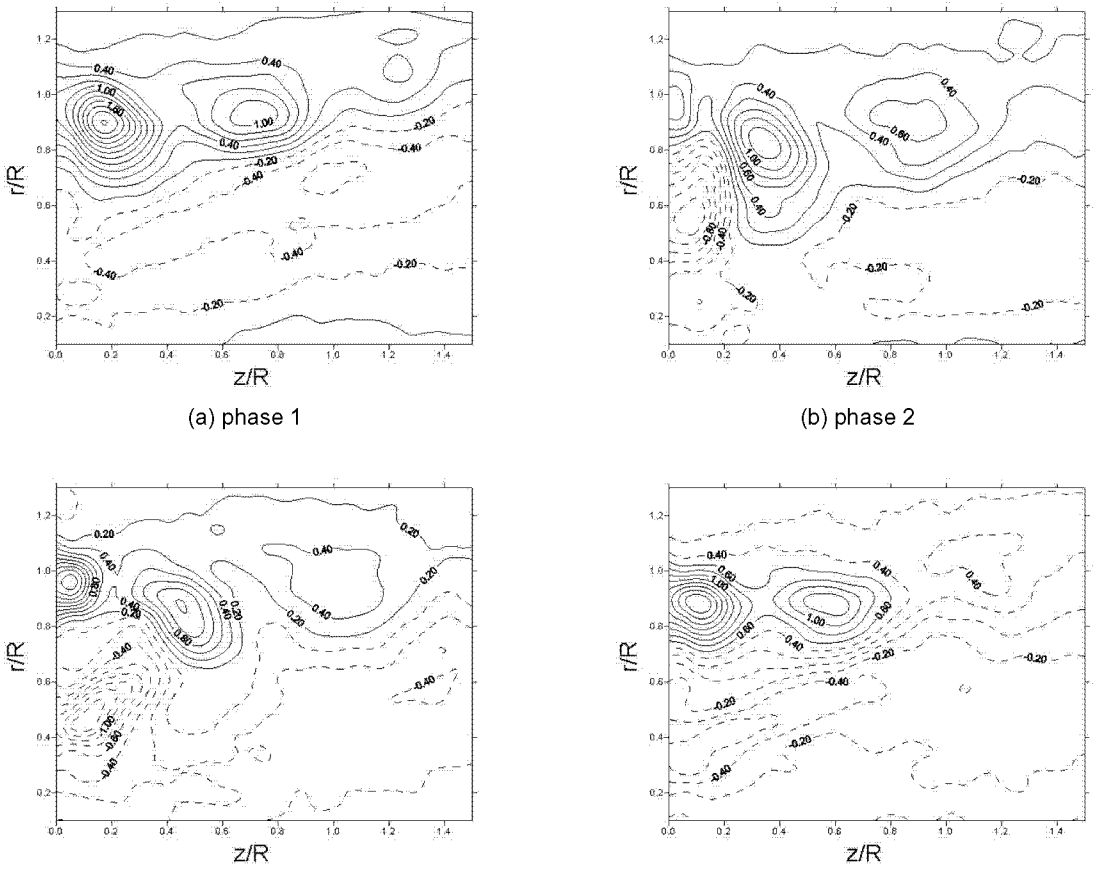

(a) phase 1 (b) phase 2

(c) phase 3 (d) phase 4

Fig. 5. Vorticity contours in the axial plane (units: s^{-1}).

is shed from the blade tip region. When the positive vortex in phase 1 moves downstream, the vorticity value is decreased.

In phase 4, the tip vortex shedding from the previous phase is moved downstream and the trailing vortex located in the lower half region in phase 3 is elongated. Such an elongation of the trailing vortex makes the flow structure in the vicinity of the hub complex. The convection velocity of the tip vortex was estimated to be about 350 mm/s, corresponding to $0.557U_{tip}$ in the axial direction.

Figure 6 shows the phase-averaged velocity fields at the mid- and tip-planes. There is relatively high-speed flow diagonally rising from the lower part of the flow field toward the blades, which keeps flowing in the diagonal direction after passing the trailing edge. The dominant flow is perpendicular to the blade surface. At the mid-plane, the dominant uprising flow changes its flow direction in the vicinity of $(z/R, r/R) = (0.3, 0.3)$. In the tip-plane, an influx is observed from the lower part of the flow field under the blade, which follows the trailing edge of the blade along the circumference of the fan. In addition, the uprising flow along the $z/R = 0.3$ line merges with the main flow rising diagonally from the blade surface to form a sink at the location $(z/R, r/R) = (-0.1, 0.4)$.

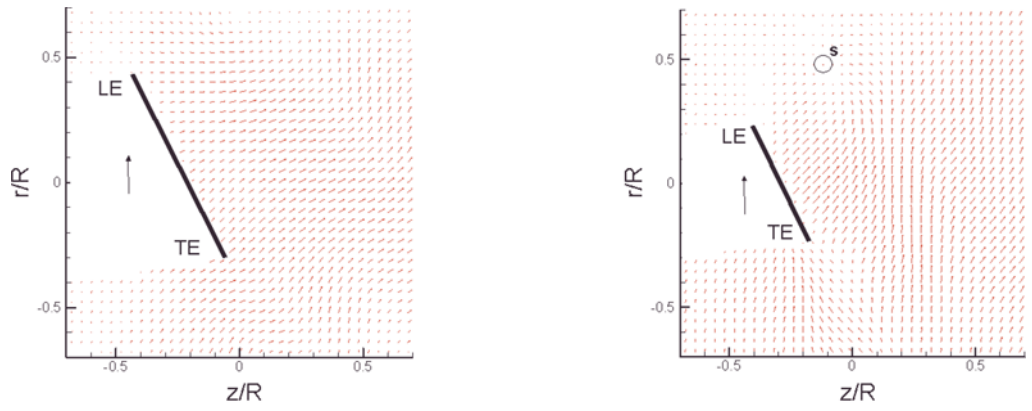

(a) mid-plane (b) tip-plane

Fig. 6. Mean velocity vector fields in the mid- and tip-planes.

The vorticity contours of the mid- and tip-planes are shown in Fig. 7. As anticipated from the velocity field results, the vorticity distribution in the tip-plane shows a higher complex flow structure compared to the mid-plane. The two vorticity contours display significantly different spatial distributions, despite the small gap distance of 8.925 mm. In Fig. 7(a), a negative trailing vortex is formed near the trailing edge of the fan blade. It is interesting to note a negative vortex centered at $(z/R, r/R) = (-0.05, 0.6)$, which is presumed to be the trace of the trailing vortex shedding from the preceding blade.

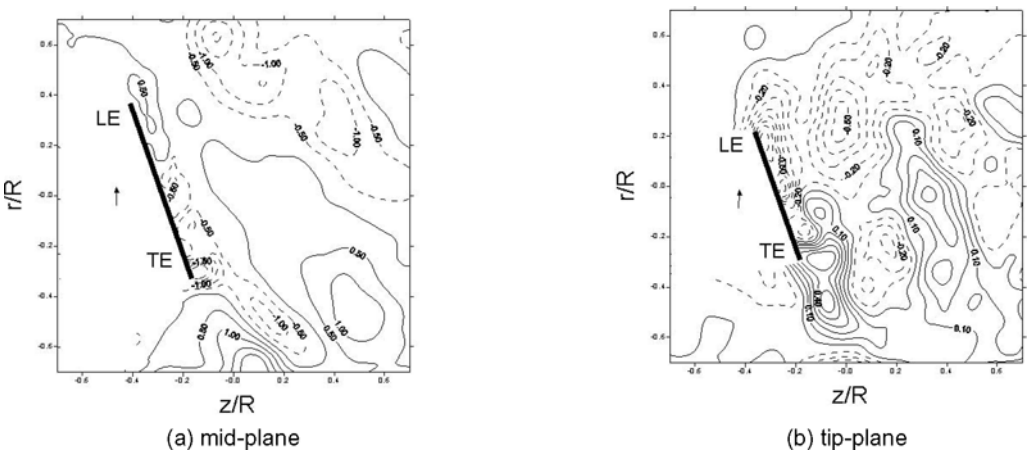

(a) mid-plane (b) tip-plane

Fig. 7. Vorticity contours in the mid- and tip-planes (units: s^{-1}).

Figure 7(b) represents the vorticity contour at the tip plane. Negative vortices rotating clockwise are distributed along the upper surface. Strong positive vortices exist at the trailing edge of the blade tip, which seems to indicate the shedding of the tip vortices. The shedding of the tip vortices can also be confirmed from the existence of the positive vortices located on the $z/R = 0.4$ line, which seems to be the trace of the tip vortex formed from the preceding blade.

3.2 Radial Planes

Figure 8 shows the phase-averaged velocity fields measured in the cross-sections perpendicular to the axis of rotation at three downstream locations ($z/R = 0.04$, 0.25 and 0.75). The axial fan is rotating in the counter-clockwise direction and the angular position of the fan blade was phase-locked such that two blades are in symmetry with respect to the vertical line $x/R = 0$, as shown in Fig. 3(c). These velocity field results clearly show the swirling flow motion as well as the decay of velocity components as the flow goes downstream.

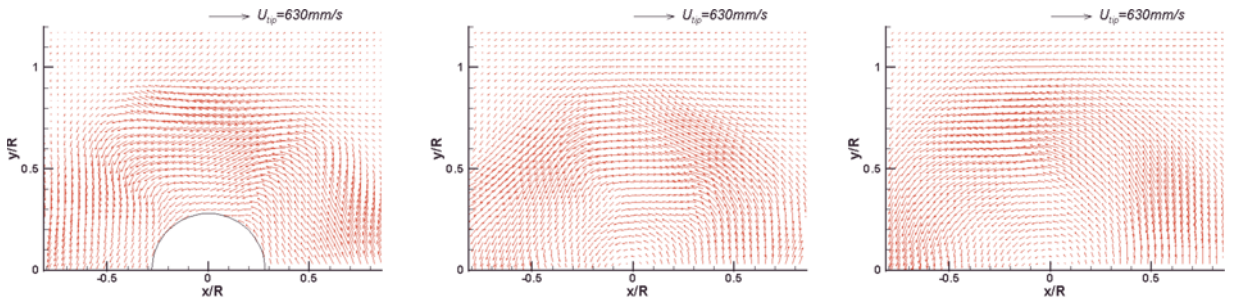

(a) z/R=0.04 (b) z/R=0.25 (c) z/R=0.75

Fig. 8. Mean velocity vector fields in the radial planes.

Figure 8(a) displays the phase-averaged velocity field at the $z/R = 0.04$ plane. In the region just behind the blade spacing between two adjacent blades, the radial velocity component is small throughout the whole radius of the fan blade. It is also interesting to note that the flow direction is drastically changed at the blade spacing. The flow velocity at the leading edge of the blade is smaller than that in the vicinity of the trailing edge. This indicates that the flow is accelerated from the leading edge to the region where the blade spacing is located. At the blade spacing, the radial velocity component is largely decreased, which may be due to the effect of blade geometry: the forward swept geometry of the fan blade pushes the flow entering the blade spacing to accelerate toward the trailing edge as the fan rotates. The maximum flow speed occurs around the points $(x/R, y/R) = (0.1, 0.7)$, (0.75, 0.1) and (–0.55, 0.4), where the blade trailing edges are located. This is in good agreement with the results measured in the axial planes. The tangential velocity component has small values in the vicinity of the hub. With increasing the radial distance from the hub, the tangential velocity component increases and has a local maximum value at $r = 0.7R$, then starts to decrease as it approaches the blade tip.

In subsequent measurement planes located further downstream, the distinctive regions having large velocity components are decreased in size and magnitude. At the $z/R = 0.25$ plane, the overall flow structure is observed to be rotated about 45° in the counter-clockwise direction with a small decay in magnitude, compared with that in the $z/R = 0.04$ plane. In Fig. 8(c), however, the regions of large radial and tangential velocity components are decreased considerably in size and no distinguished flow structure exists. The vector field shows a spiral motion with a vague periodic flow structure at further downstream locations. The radial velocity component is increased as the distance from the hub increases. From the velocity fields measured in the radial planes, the local maximum velocity was located around the circumference of a circle with radius $0.7R$.

In the vorticity contour plots shown in Fig. 9, the red color represents positive counter-clockwise vortices and the blue color represents negative clockwise vortices. At the radial plane $z/R = 0.04$, the negative vortices around the blade tips represent the tip vortex. The elongation along the blade tips is due to the forward-swept geometry of the fan blade, forming a large roll-up region for the scraping vortices at the blade tips. The positive trailing vortices are also elongated along the fan blade. These seem to be caused by merging and interaction of the two boundary layers developed on the upper and lower surfaces of each fan blades. The tip vortex and the trailing vortex seem to shed alternately. As the flow moves downstream, the angular distance between the trailing vortices and the tip vortices is changed continuously and the strength of the two vortices is decreased.

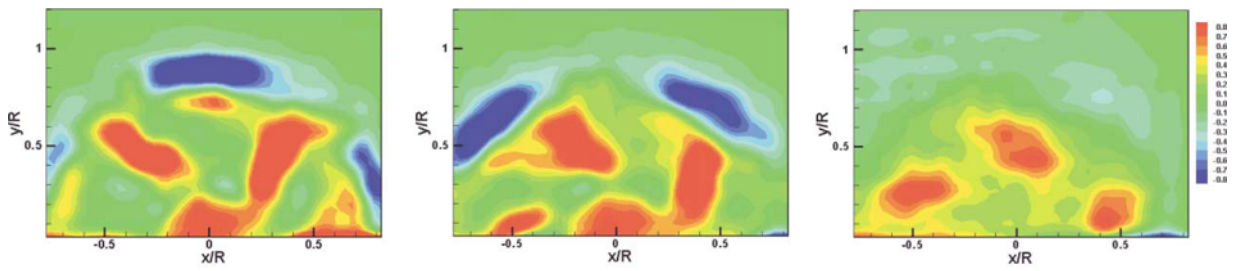

Fig. 9. Contour plots of mean vorticity in the radial planes (units: s^{-1}).

From these contour plots, we can see that the angular convection velocities of the two vortices are different and that the tip vortex is dissipated faster than the trailing vortex. The tip vortex has a slightly higher initial vorticity compared with the trailing vortex at the $z/R = 0.04$ plane. In the $z/R = 0.75$ plane, however, it is difficult to find the tip vortex, and only weak trailing vortices generated from the fan blades are observed. From these results, we can see that the tip vortex has a higher decay rate compared to the trailing vortex. This may result from the difference in moving distance of the two vortices; the tip vortex moves a relatively long distance compared with the trailing vortex located near the hub, in addition, the tip vortex is subject to a larger centrifugal force from the fan rotation.

4. Conclusions

The flow structure of turbulent wake behind an axial fan has been investigated experimentally using a phase-averaged 2-frame PTV technique. The axial fan with 5 blades was rotated at 240 rpm and velocity field measurements were carried out at 4 axial planes and 4 radial planes. For each measurement plane, 500 instantaneous velocity field data were obtained and ensemble averaged to obtain the phase-averaged velocity fields and vorticity contours. The wake flow behind the axial fan has a periodic flow structure according to the blade phase, and the flow pattern in each phase is shifted downstream in the next phase. Strong vortices rotating in the counter-clockwise direction are shed from the trailing edges of the blade and the convection velocity of the vortices is found to be about $0.557U_{tip}$ in the axial direction. The tangential velocity component is accelerated as the flow goes from the leading edge to the trailing edge of the blade, while the radial velocity component is directed toward the hub. The tangential velocity component has maximum values in the radial distance of about $r=0.7R$. Clockwise tip vortices are shed from the blade tips, while counter-clockwise trailing vortices exist near the hub region. The tip vortex has a higher decay rate than the trailing vortex.

Acknowledgments

This study was partially supported by the National Research Laboratory program and LG Electronics.

References

Baek, S. J. and Lee, S. J., A New Two-frame Particle Tracking Algorithm Using Match Probability, Experiments in Fluids, 22 (1996), 23-32.

Cotroni, A., Felice, F., Romano, G. P. and Elefante, M., Investigation of the Near Wake of a Propeller Using Particle Image Velocimetry, Experiments in Fluids, 29 (2000), S227-S236.

Inoue, M. and Kuroumaru, M., Three-dimensional Structure and Decay of Vortices behind an Axial Flow Rotating Blade Row, Journal of Engineering for Gas Turbines and Power, 106 (1984), 561-569.

Lee, S. J. and Lee, S. H., Synchronized Smoke-wire Technique for Flow Visualization of Turbulent Flows, Journal of Flow Visualization and Image Processing, 6 (1999), 65-78.

Morris, S. C., Good, J. J. and Foss, J. F., Velocity Measurements in the Wake of an Automotive Cooling Fan, Experimental Thermal and Fluid Science, 17 (1998), 100-106.

Ravindranath, A. and Lakshminarayana, B., Mean Velocity and Decay Characteristics of the Near and Far-wake of a Compressor Rotor Blade of Moderate Loading, Journal of Engineering for Power, 102 (1980), 535-548.

Reynolds, B. and Lakshminarayana, B., Characteristics of the Neak-wake of a Compressor or Fan Rotor Blade, AIAA Journal, 17 (1979), 959-967.

Schmidt, D. P. and Okiishi, T. H., Multistage Axial-flow Turbomachine Wake Production, Transport and Interaction, AIAA Journal, 15 (1977), 1138-1145.

Sinha, M. and Katz, J., Flow Structure and Turbulence in a Centrifugal Pump with a Vaned Diffuser, Proc. of 1998 ASME Fluids Engineering Division Summer Meeting (Washington DC), (1998-6), FEDSM98-5129.

Author Profile

Sang Joon Lee: He received his master and Ph.D degrees in Mechanical Engineering from KAIST (Korea Advanced Institute of Science and Technology) in 1982 and 1986, respectively. In 1986 he worked as a senior researcher at KIMM. He is currently a professor in the Department of Mechanical Engineering at POSTECH after joining as an assistant professor in 1987. His research interests are quantitative flow visualization (PIV, PTV, LIF, Holography), experimental fluid mechanics, bluff body aerodynamics, microfluidics and flow control.

Jayho Choi: He received his MS degree from POSTECH in 2000 and is currently a research engineer at LG Electronics. His research interest is in the development and application of PIV system in microfluidics.

In Seop Lee : He received his MS degree in Mechnical Engineering in 1989 at Kyunghee University and Ph.D in 1999 in Environmental Engineering at Osaka University. He started his research career as a research engineer at LG Digital Appliance Research Laboratory. His research interests cover flow visualization, PIV, microfluidics and flow control.